Comparative Analysis of Synthesis Routes for Antimony-Doped Tin Oxide-Supported Iridium and Iridium oxide Catalysts for OER in PEM Water Electrolysis

Marius Gollasch, Jasmin Schmeling, Corinna Harms,* and Michael Wark

This study investigates and compares four different deposition methods for an iridium-based catalyst on antimony-doped tin oxide support for oxygen evolution reaction in water electrolysis. Different synthesis routes often lead to varying properties of the resulting catalyst and can result in performance disparities. Here, some of the most prominent methods are carried out on the same support material and evaluated with special focus on the deposition yield of Ir and thus cost efficiency along with electrochemical performance. The catalysts are also assessed based on their chemical composition, namely Ir or IrO_2-based, with an additional thermal treatment to convert Ir to IrO_2 species. The chosen synthesis routes result in different Ir species to obtain tetragonal IrO_2 a modified Adams fusion approach delivers the best controllable and highest Ir loading and thus superior electrochemical performance. As far as metallic Ir catalysts are concerned, a wet-chemical reduction-based synthesis results in the most desirable catalyst, which however falls behind the Adams fusion catalyst upon thermal treatment to IrO_2. The work in this study is a comprehensive analysis of different synthesis influences and recommends practices for laboratory-based syntheses and an outlook on industrial viability.

1. Introduction

The transition of the energy system from a fossil fuel-based one to renewable and green energy carriers is one of the main challenges in the coming years. With H_2 being a promising carrier, its generation and conversion pose technological demands. The generation of H_2 is possible in different processes like the steam reforming of hydrocarbons, currently used in industrial processes or electrolysis of water.[1,2] In terms of electricity generation and utilization of H_2 as fuel in transportation, the latter approach seems to be opportune to minimize the reliance on fossil fuels and curb CO_2-emissions.[1,3] With electrolysis, the generated H_2 could help establish a carbon-neutral transportation system. Additionally, in combination with fuel cells it can act as quasi-energy storage, both short- and long-term, to balance temporal disparities in the generation of renewable energy.[4–6]

One implementation of water electrolysis is its proton exchange membrane (PEM) variant, which utilizes a proton-conducting polymer membrane and noble-metal catalyst electrodes.[1] These catalysts are most often made from Pt on the cathode side and Ir on the anode. Noble metals are to some extent necessary here especially for the anode since the chemical environment presents harsh conditions and high oxidizing potentials, making most catalyst materials unstable long-term. Utilization of Ir comes with the downside of high investment costs, due to scarcity of Ir and therefore high price, which hinders the widespread application of PEM electrolysis systems.[1,3,6] In 2020 alone, the price of Ir tripled.[1,3] Reduction of the overall Ir content in PEM electrolysis systems is thus paramount for further industrial implementation. Recently, most employed catalysts consist either of metallic Ir, so-called Ir black or IrO_2 but these offer quite low volumetric activity, due to their nature as bulk catalysts. One strategy to reduce the Ir loading is to attach the catalyst to a conductive support material, quite similar to already applied fuel cell catalysts, with Pt supported on C.[7–9] In PEM electrolysis, the support also has to withstand harsh conditions, and thus the choice of material is drastically narrowed. Some metal oxides, like TiO_2, are stable at the anode; however, their electrical conductivity is several orders of magnitude lower than that of bulk Ir; thus, the overall current efficiency is diminished.[7] Doping of the metal oxide lattice can alleviate the conductivity problem. One of the most promising candidates is antimony-doped tin oxide (ATO), which shows adequate electrical conductivity and stability.[10–15] Moreover, ATO might induce positive effects into Ir catalyst species, for instance,

M. Gollasch, C. Harms
German Aerospace Center (DLR) e.V.
Institute of Engineering Thermodynamics
Carl-von-Ossietzky-Str. 15, 26129 Oldenburg, Germany
E-mail: corinna.harms@dlr.de

J. Schmeling, M. Wark
Institute of Chemistry, Chemical Technology 1, Carl von Ossietzky
University of Oldenburg
Carl-von-Ossietzky-Str. 9-11, 26129 Oldenburg, Germany

enhanced stability or activity.[16–18] Ir is deposited on the support material and its chemical composition can vary depending on the synthesis route. Metallic Ir catalysts are electrochemically oxidized under operation conditions to form a mixed oxide IrO_x layer.[19,20] This species shows the highest activity toward oxygen evolution reaction (OER); however, it exhibits performance decay, due in part to lattice defects. On the other hand, thermally treated Ir is converted to crystalline tetragonal IrO_2 and shows enhanced stability, especially during long-term operation, but lower performance.[19,21–23] In addition to the oxidation state of Ir, several other factors are influenced by the synthesis, such as Ir particle dispersion and size. Scalability of reaction schemes for industrial applications and efficiency regarding Ir deposition yield influence the choice of synthesis route.

Here, we present a comparative analysis of different synthesis routes for ATO supported Ir catalysts regarding their physical characteristics as well as electrochemical performance. Catalysts are produced via i) $NaBH_4$ reduction, ii) modified Adams fusion reaction and, iii) polyol synthesis with two different ATO deposition techniques, namely colloidal and hydrothermal deposition.[7,8,24–26] The produced Ir@ATO catalysts, containing non-IrO_2 species, that is, metallic Ir or IrO_x, are also calcined in an additional step to convert them to IrO_2, which promises increased stability.[19,21–23]

2. Results and Discussion

2.1. Iridium Loading

Catalysts were prepared in three different theoretical loading variants consisting of relatively high, medium, and low amounts of Ir with 65, 40, and 15 wt%, respectively. For the synthesis of catalysts, especially those involving noble metals, the yield of active material is very important as low deposition yield can often result in noble metal losses or costly recovery steps. To evaluate the deposition yield, all catalysts were dissolved and subsequently analyzed using inductively coupled plasma-mass spectrometry (ICP-MS) and the results are shown in **Figure 1**. Four synthesis routes were compared, namely reduction synthesis by $NaBH_4$ (RS), modified Adams fusion method (MAF), colloidal deposition by precipitation of an Ir particle suspension (CD), and hydrothermal deposition involving tert-butanol (HTD).
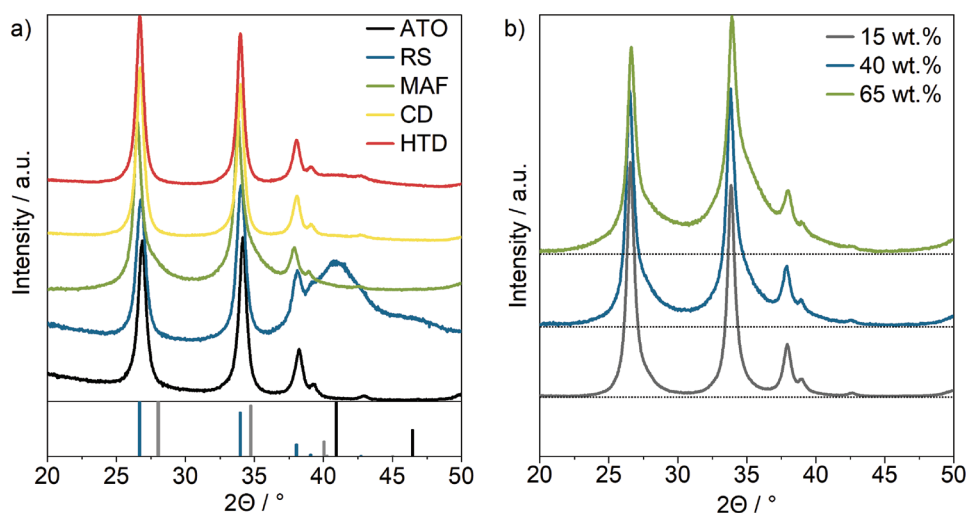
All syntheses were carried out twice to determine reproducibility, however, the second syntheses for CD and HTD with 15 and 65 wt% loading resulted in insufficient material for ICP-MS analysis and were thus omitted. RS showed the overall highest deposition yields and highest reproducibility with both attempts showing an Ir loading within ± 2 wt% of the desired loading. Wang et al. showed with the same synthesis procedure an Ir loading of only 24 wt% with intended 30 wt% on Ti_4O_7 support.[24] The increased yield reported here might indicate a favorable impregnation or interaction of the ATO support and the $IrCl_3$ precursor and thus higher reduction conversion by $NaBH_4$. Catalysts synthesized according to the MAF method showed loadings slightly below the desired ones in the first attempt ranging from 8 to 12 wt% lower loading. However, the second attempt led to loadings within the margin of error of
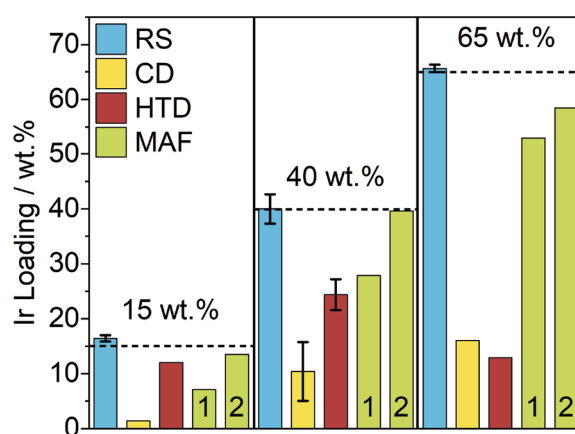
Figure 1. Ir loading depending on catalysts with indicated desired loadings of 15, 40, and 65 wt% (Ir@ATO) based on catalyst digestion and ICP-MS analysis. Error bars are indicated for repeated measurements with the exception of MAF synthesis which is indicated with first and second synthesis as discussed below.

the desired loading, comparable to the RS method. Here, the impregnation step of ATO with precursor and $NaNO_3$ was prolonged from 30 min to 3 days and a tip-sonication step was implemented. Dispersion and complete dissolution of $IrCl_3$ thus seem to be important for complete oxidation and subsequent deposition of the support. Due to the relatively simple nature of the synthesis, this method presents a strong contender for the synthesis of choice for laboratories since the loading is also targetable in the right conditions as shown in the second synthesis attempt.

CD and HTD syntheses were both performed with the same colloidal Ir suspension, however, they differ substantially in the final Ir loading. The CD method shows very low loading across all syntheses. Similar methods from the literature provide some explanations as Hartig–Weiss et al.[25] presented catalysts with only half the intended loading, while Abbou et al.[26] obtained loadings relatively close to the desired one. In general, this method seems to be very dependent on specific factors in the synthesis, such as the specific surface area of the support where a higher area leads to a more complete deposition.[26] The surface area of the ATO support, reported here, is around 28 cm^2 g^{-1}, which could be the reason for low CD loading since deposition was significantly higher on ATO aerogels with surface areas between 40 and 80 cm^2 g^{-1}.[26] The loss of Ir particles seems substantial and it can most likely not be recovered directly or requires great effort, as the Ir is already in nanoparticle form and hence prone to agglomeration. Comparison to HTD, however, indicates low nanoparticle deposition as the main problem for CD since HTD with the same colloid suspension results in higher loadings for 15 and 40 wt% catalysts. Low depositions for both syntheses for 65 wt% indicate an incomplete reaction during the colloid formation, which underlines the unreliability of this specific method. With better reproducible colloid formation routes, HTD shows promise to provide reliable Ir loadings as described by Böhm et al. who obtained nearly quantitative deposition with this synthesis.[8] The differing amounts of Ir deposited for CD and HTD across all catalysts are supposedly due to incomplete formation of Ir

**ADVANCED
SCIENCE NEWS**

www.advancedsciencenews.com

**ADVANCED
MATERIALS
INTERFACES**

www.advmatinterfaces.de

Figure 2. a) Diffractograms of all synthesis methods in 40 wt% desired Ir loading and pristine ATO as a reference with indicated reflexes for cubic Ir (black, ICDD: 00-046-1044), tetragonal IrO_2 (gray, ICDD: 00-015-0870) and ATO ($Sb_{0.1}Sn_{0.9}O_2$, blue, ICDD: 98-015-5956). b) Diffractograms of MAF synthesis method with different desired Ir loadings.

colloid and then again incomplete deposition of said colloid on the support for the CD method.
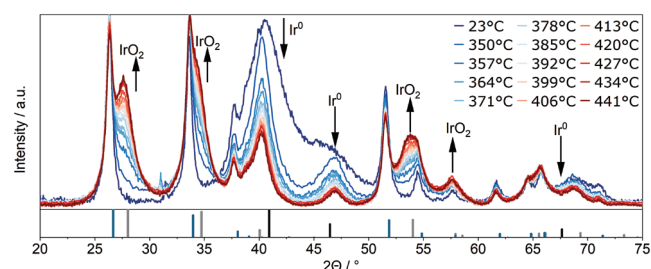
2.2. Morphology and Chemical Composition

Reduced diffraction angle diffractograms for better reflex resolution of the different synthesis routes are shown in **Figure 2**a along with line-diffractograms as reference. Full angle diffractograms are presented in Figure S2, Supporting Information. Most prominently, RS shows a strong peak at around 41.0° 2Θ, which can be assigned to cubic Ir^0(111) and is the main indicator for the presence of metallic Ir.[8,24,27] Additional Ir^0 reflexes can be assigned to 46.5, 67.7, 81.9, and 86.4° 2Θ (Figure S2, Supporting Information), which correspond to the Ir^0(200), (220), (311) and (222) crystal faces, respectively.[8,24,27] However, the minor reflexes at higher diffraction angles are not distinguishable from the ATO signals due to their low relative intensity. The strong reflexes at 41.0 and 46.5° 2Θ suggest a predominant presence of metallic Ir, with no indication of crystalline oxidic forms. The reflexes at 41.0 and 46.5° 2Θ are quite broad, implicating small crystallites and supposedly small particles. Scherrer analysis of this peak results in a relatively low crystallite size of 1.7 nm. However, many reflexes overlap in these samples, which is why a crystallite size determination according to Scherrer is non-trivial and the values presented here are rough estimate. These reflexes are also present in HTD, albeit at a much smaller intensity, indicating small amounts of Ir present in cubic Ir^0 since the overall Ir loading is not substantially lower than RS to cause such low reflexes. This suggests that the Ir present in HTD may be in another oxidation state or that it is not present in a sufficiently large crystalline form. Böhm et al. also report a broad reflex corresponding to cubic Ir^0 at 41° 2Θ, which implies fairly small crystallites and ATO reflexes shown here may overlap the very broad reflex from cubic Ir^0.[8] The diffractogram of CD shows no substantial reflexes besides ATO ones. This is in agreement with literature results, where no reflexes can be observed for similar

catalysts.[26] Yet, for other colloidal synthesis methods, a signal around 33° 2Θ was observed, which corresponds to hydrous IrO_x.[8] The absence of this signal could imply an amorphous character of Ir species present in the CD method because only crystalline species generate peaks in diffractograms. In contrast, the diffractogram for MAF catalyst shows strong tailings of the ATO reflexes at 28.0 and 34.8° 2Θ, indicating tetragonal IrO_2 and correspond to IrO_2(110) and IrO_2(101), respectively.[8] These diffractions are only visible in the MAF sample indicating no IrO_2 presence in the other samples. Additionally, Scherrer analysis results in a tetragonal IrO_2 crystallite size of 2.0 nm since these reflexes are quite broad and thus corroborate limited particle growth at the chosen MAF reaction temperature of 375 °C. Compared to a lower reaction temperature of 350 °C, the crystallite size increases only slightly from 1.7 nm, as reported by Abbot et al., to 2.0 nm observed here.[28] Interestingly, between 350 and 375 °C, different IrO_2 facets emerge as no (110) at 28.0° 2Θ and (211) at 54° 2Θ (Figure S2, Supporting Information) are visible at the lower temperature, whereas they appear at the higher one.[28,29] Since rod-like tetragonal IrO_2 gets formed along the (110) plane, on-setting crystal growth for this structure can be observed between 350 and 375 °C.[28] Other studies using this synthesis method report higher crystallite sizes for higher temperatures, as expected, for example, 5.0 nm at 500 °C.[13,28]

Comparing the diffractograms of different loadings of one synthesis, increasing Ir reflexes become clear, as presented in Figure 2b. Here, the IrO_2 reflexes at 28.0 and 34.8° 2Θ gain intensity with higher loading, as expected. With higher loading, the crystallite size of these reflexes decreases from 2.9 to 2.0 to 1.7 nm. One explanation could be higher crystallization through oxidation since the ratio of oxidant $NaNO_3$ to precursor $IrCl_3$ is highest at 15 wt% and decreases to higher loadings. This suggests that not only the reaction temperature but also the $NaNO_3/IrCl_3$ ratio plays a significant role in particle formation even at an overall excess of oxidant. For other synthesis methods, this trend is also not apparent, as the RS crystallite size remains constant for different loadings.

2300036 (3 of 12)

**ADVANCED
SCIENCE NEWS**

www.advancedsciencenews.com

**ADVANCED
MATERIALS
INTERFACES**

www.advmatinterfaces.de

Figure 3. In situ high-temperature diffractogram for 65 wt% loaded RS catalyst with indicated peaks corresponding to cubic Ir and tetragonal IrO_2 and intensity trends with indicated reflexes for cubic Ir (black, ICDD: 00-046-1044), tetragonal IrO_2 (gray, ICDD: 00-015-0870), and ATO ($Sb_{0.1}Sn_{0.9}O_2$, blue, ICDD: 98-015-5956). Color grading indicates the calcination temperature for blue at room temperature to red at 441 °C with 7 °C steps from 350 to 441 °C.

Upon thermal treatment in air at 375 °C for three of the four methods, namely RS, CD and HTD, since MAF is already in IrO_2-form, the observed reflexes shift to those corresponding to tetragonal IrO_2. To elucidate the calcination process at different temperatures, in situ high-temperature X-ray diffraction (XRD) was carried out, where the temperature ramped up step-wise with a synthetic air atmosphere. The results are shown in **Figure 3**.

As expected, Ir^0 reflexes decrease in intensity and IrO_2 ones increase. Already at 350 °C, a small increase can be observed at 28.0 and 34.8° 2Θ, and more apparent the cubic Ir reflex at 41.0° 2Θ shrinks but also becomes narrower. This narrowing for this reflex only occurs once between room temperature and the first heating step and can be attributed to particle growth with only minimal oxidation. With higher temperatures the reflex shift continues, while the Ir(111) reflex does not narrow further but only decreases in intensity. The largest intensity decrease of the Ir reflex happens between room temperature and 380 °C and slows down afterward, indicating the majority of oxidation takes place at comparatively low temperatures. Nevertheless, complete oxidation to IrO_2 does not take place at temperatures below 400 °C even after hour-long treatment.[30] Interestingly, the apparent intensity of the IrO_2 reflex at 28° 2Θ increases more than the Ir one decreases, which could be explained by further crystallization of IrO_2 from amorphous or polycrystalline oxide and thus narrowing of the reflex. Higher crystallinity of IrO_2 increases its electrochemical stability but also dampens activity.[19,21] The chosen temperature at 375 °C, as suggested by Böhm et al., does seem to invoke the majority of Ir oxidation, while preserving low crystallinity of IrO_2, improving its electrochemical activity, and preserving disperse small particles to improve activity even further.[8] Trends observed in the high-temperature diffractograms can also be seen in thermally treated catalysts, with Ir(111) narrowing and the emergence of IrO_2 reflexes in calcined RS catalysts. Ir(111) crystallite sizes for the 40 wt% calcined RS sample (Table S2, Supporting Information) increases substantially from 1.7 to 5.3 nm upon calcination, while tetragonal IrO_2 crystallites display around 2.8 nm sizes, slightly bigger compared to MAF catalysts. Considering the growth of crystallite size below 350 °C, as shown in Figure 3, calcined catalysts might experience Ir particle ripening first and oxidation of the surface to IrO_2 second. The same shifts from Ir to IrO_2 can also be observed for the HTD sample (Figure S3a, Supporting Information), however, the Ir(111) reflex becomes almost indistinguishable, which could be due to the already very low intensity of this reflex in the uncalcined sample. CD (Figure S3b, Supporting Information) only shows an emergence of IrO_2 reflexes upon calcination and no shift for others.

Transmission electron microscopy (TEM) micrographs of selected calcined and uncalcined catalysts are displayed in **Figure 4**.
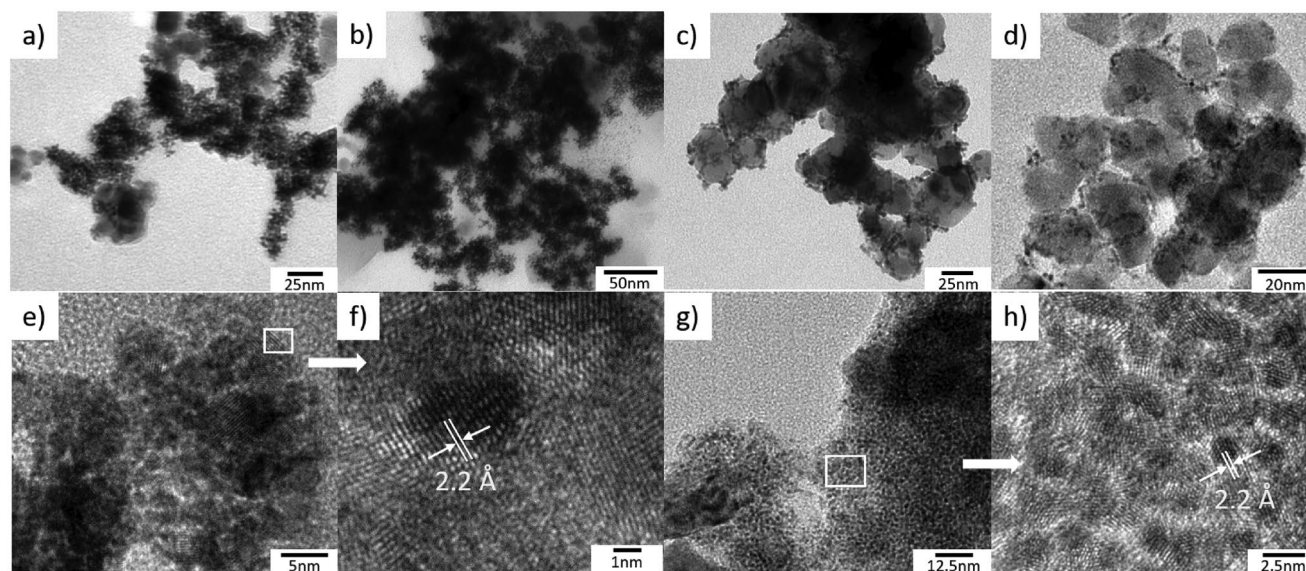
Figure 4. TEM micrographs of a) uncalcined 40 wt% Ir RS catalyst, b) uncalcined 65 wt% Ir RS catalyst, c) uncalcined 40 wt% Ir HTD catalyst, d) uncalcined 40 wt% Ir CD catalyst, e,f) calcined 65 wt% Ir catalyst with enhanced resolution and indicated particle lattice spacing in (f,g) and h) MAF 65 wt% Ir catalyst with enhanced resolution and indicated particle lattice spacing in (h).

2300036 (4 of 12)

At medium loading of 40 wt% RS method (Figure 4a) shows an extended network of Ir particles on the support, while individual particles are still distinctly visible. They are however not uniformly distributed, since ATO without Ir is still visible. Agglomeration of particles is normally a disadvantage because active surface area is lost where particles touch. Nevertheless, the formation of a percolating network can be beneficial in the case of electrolysis since the electrical conductivity could be enhanced.[7,8] Electrical pathways would in this case lead through the Ir particle network with significantly higher conductivity compared to the ATO support. This network phenomenon can also be observed at lower loading of 15 wt% (Figure S5, Supporting Information) but individual patches of particles might be too isolated to form a percolation network. Here, the clustering of particles might be a disadvantage since the surface area is reduced without the benefit of a conducting network. At higher loading of 65 wt% (Figure 4b) the significance of reduced surface area might come into effect since the support is no longer visible and completely covered with Ir particles. A higher surface area of the support could alleviate this problem and allow higher loading with more capacity for Ir particles but the ATO support presented here seems to have an optimal loading between 40 and 65 wt% Ir considering RS method. The optimal loading thus also depends on the support surface area and will most likely deviate from the results shown here between 40 and 65 wt% Ir. When calcined, the Ir particles become brighter in TEM micrographs and therefore become harder to identify on ATO support due to the lower electron density in IrO_2.[11] Figure 4e shows the support uniformly covered with mostly larger particles compared to the uncalcined sample, which is in line with the higher crystallite size observed in XRD. Smaller individual particles are however visible at higher magnification (Figure 4f), which show a lattice spacing of 2.2 Å that points to both metallic Ir (111) and IrO_2 (110).[8,17,31] The darker particle visible is most likely metallic Ir considering the greater contrast with IrO_2 surrounding it.

In contrast to RS, the HTD sample shown in Figure 4c displays individually dispersed Ir particles. They seem to uniformly cover the support with only very small clusters of particles visible. The relative available surface area of Ir particles might be higher here compared to RS if the particles have the same size but the lack of percolating particles might hinder its performance in a membrane electrode assembly (MEA) setup. With a more conductive support material compared to ATO, this method might however be advantageous to RS considering the dispersement of particles. As the support material is visible, the loading capacity might also be higher here and the addition of more Ir could induce percolating effects at a certain threshold. Similarly dispersed are the particles on the support in the case of CD in Figure 4d. Morphologically, both HTD and CD catalysts seem similar even though the actual loading is quite different as discussed above. IrO_2 particles in the MAF catalysts are uniformly dispersed across the whole support as seen in Figure 4g. They are arranged in a film-like nature composed of very small particles, which corroborates the small crystallite sizes observed from XRD analysis. The individual particles also display a lattice spacing of 2.2 Å that corresponds to either cubic Ir or tetragonal IrO_2 and thus
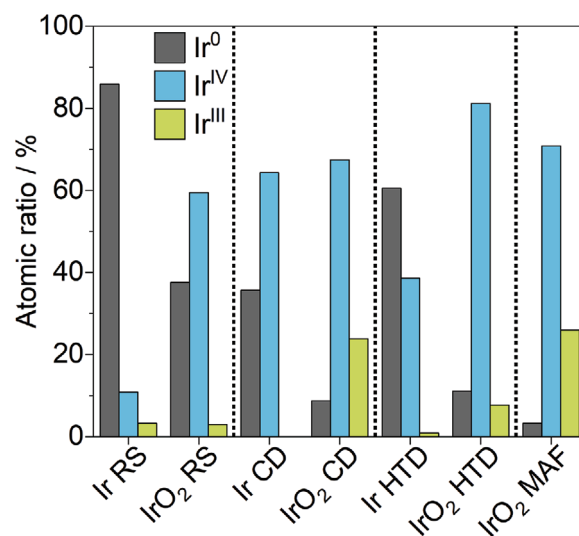

Figure 5. Comparison between the chemical composition of Ir4f species detected by XPS and indicated in the atomic ratio between different oxidation states for uncalcined and calcined catalysts.

affirms the particles being IrO_2 since no cubic Ir was detected in XRD.[17,31]

For further investigation into the chemical composition of the Ir catalysts, X-ray photoelectron spectroscopy (XPS) was carried out and an overview of Ir4f spectra fitting is shown in **Figure 5** and the spectra are displayed in **Figure 6**. Analysis of O1s spectra in correlation to Ir species was not possible and is omitted due to the overshadowing amount of O bound in the ATO support material.

As suggested by diffractograms of RS catalysts, the majority of Ir is composed of Ir^0 with negligible amounts of Ir^{IV} most likely due to minor surface oxidation in ambient air.[24] Upon calcination this signal shifts to higher amounts of Ir^{IV}, however Ir^0 is still preserved, which is in accordance with diffractograms as not all Ir^0 is oxidized. The presence of Ir^0 in XP spectra might still not dampen long-term stability, since Ir^0 could still be observed in XPS with electrochemically oxidized samples. This suggests the detection in deeper layers that are not electrochemically available.[25] With depth sensitivity of XPS depending on the mean free path of electrons, the escape depth of electrons is much higher for Ir than the particle size and thus detection of the whole particle is possible.[32] Oxidation only on the surface of the Ir^0 particles during calcination may lead to a core-shell-like structure with Ir^0 still present in the core. Ir^{III} amounts stay negligibly low also after oxidation, which suggests oxidation of Ir metal directly to Ir^{IV}. Additionally, Pfeifer et al. observed a low presence of Ir^{III} in amorphous IrO_2, which can also be observed in oxidized RS samples and thus would indicate amorphous IrO_2 in addition to crystalline.[33] HTD employs a similar Ir deposition strategy as RS concerning the targeted Ir species, where Ir^0 is formed on the support. The XP spectrum for these catalysts confirms a majority of Ir as Ir^0, however, a substantial amount is present as Ir^{IV}, especially compared to RS. No or only a minor detection of Ir^{III} in addition to Ir^{IV} precludes IrO_x as this species is associated with a superposition of both oxidation state signals.[30]
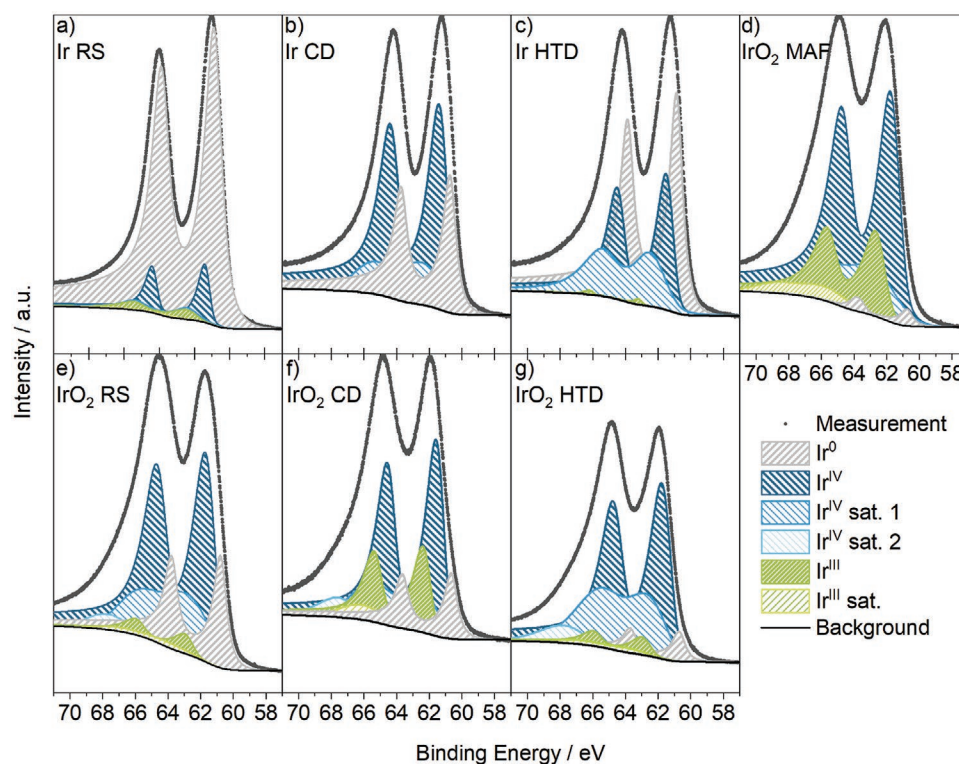
Figure 6. Ir 4f high-resolution XP spectra of a–d) uncalcined and e–g) calcined catalysts.

Thus Ir^{IV} could more likely be present as $Ir(OH)_4$, as no rutil-IrO_2 reflexes were visible in XRD.[25] This stems from incomplete reduction since Böhm et al. report higher amounts of Ir^0 for the same deposition method. Here, the colloid was prepared with a different method and the larger amounts of ethylene glycol shown here may have impacted the reduction capability of the tert-butanol.
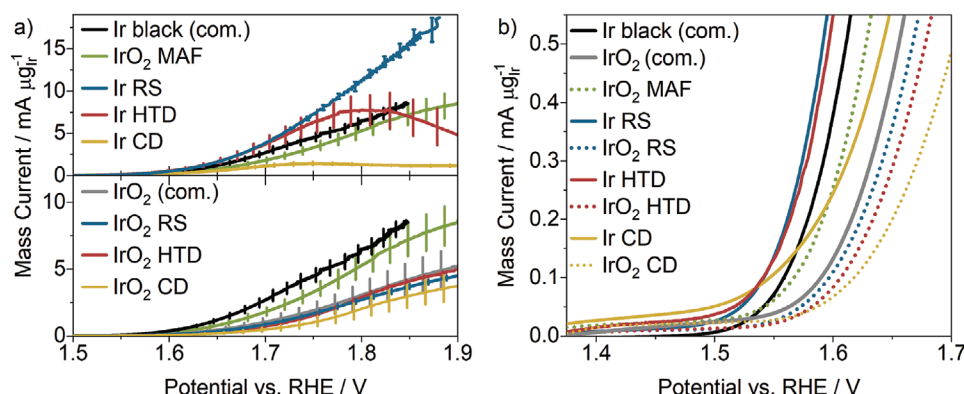
Compared to CD, which utilized the same colloid, HTD reduces Ir^{IV} upon hydrothermal treatment but overall remains almost exclusively Ir^0 and Ir^{IV} with hardly any Ir^{III} present. The absence of Ir^{III} for CD was also observed by Hartig-Weiss et al., who however detected more Ir^0 but this difference could also be due to different spectra fitting.[25] It was also observed that the oxidation state of Ir on polyol methods depends on the support material and in this case, ATO might induce a higher amount of Ir^0.[17,34] Upon calcination, the CD sample signal shifts mostly Ir^0 to Ir^{III}, which is in contrast to the calcined RS sample, which showed no shift to Ir^{III} but only to Ir^{IV}. In literature, this signal shift could also be observed but only in electrochemical oxidation without thermal treatment.[25] Calcined HTD experiences a similar signal shift in Ir species as the RS catalyst. With a higher Ir^{IV} content in the pristine sample, this species becomes the almost sole oxidation state with almost all Ir^0 being oxidized. The higher amount of Ir^{III} in addition to Ir^{IV} is also present in the IrO_2 MAF catalyst. Compared to commercial IrO_2, the MAFs Ir^{III} content is quite high since it only appears in small amounts in the commercial one.[34] Here, negligible amounts of Ir^0 are present but the high Ir^{III} presence might indicate incomplete oxidation of the Ir^{III} precursor but no Cl could be detected, indicating a complete conversion of

$IrCl_3$. Ir^{III} states in IrO_2 have been explained above and were also observed by Freakley et al.[35] Differing ratios of Ir^{IV} and Ir^{III} in RS and MAF could be the result of differing amounts of amorphous IrO_2, where MAF would show a much larger presence. Higher amounts of amorphous IrO_2 could be the result of reaction conditions, where $NaNO_3$ suppresses crystal growth more than thermal treatment. The particle size of IrO_2 in MAF is also very small, which would place more Ir atoms on the surface, which in turn could lead to higher amounts of hydroxo species and a shift toward Ir^{III} for IrO_2 crystals.[28] Alternatively, Ir^{III} presence thus might indicate some amount of a IrO_x structure, where Ir vacancies and thus superfluous electrons in the IrO_2 cell lead to a local reduction of Ir^{IV} to Ir^{III} atoms, as described theoretically by Pfeifer et al.[33] In contrast, the calcined RS is most likely just composed of metallic Ir and rutil-IrO_2 as no substantial amount of Ir^{III} is present.

2.3. Electrochemical Performance

The electrochemical activity and performance toward the OER was evaluated by half-cell rotating-disk electrode (RDE) experiments in liquid electrolyte. Comparison of different synthesis methods is in addition to the produced catalysts morphology very dependent on performance-based indicators for the desired application. In the evaluation of metallic Ir and IrO_2, the viability of the catalyst is a trade-off between intrinsic activity and its long-term stability.[19] Mass-normalized polarization curves of all catalysts are shown in **Figure 7**a and mass activity at 1.55 V versus RHE based on actual catalyst loading in **Figure 8**.

**ADVANCED
SCIENCE NEWS**

www.advancedsciencenews.com

**ADVANCED
MATERIALS
INTERFACES**

www.advmatinterfaces.de

Figure 7. Mass normalized polarization curves a) of the (upper) uncalcined catalysts and (lower) calcined catalysts with 40 wt% desired loading and Ir black and MAF catalyst as a reference and b) at a low overpotential of Ir (solid line) and IrO_2 (dotted line) catalysts with the desired 40 wt% Ir loading.

Uncalcined RS catalysts display the highest mass current across the whole potential area, even higher than the reference Ir black catalyst.

Higher performance than the reference is mostly the result of the effect of a supported catalyst, in which the available surface area of Ir particles is increased due to higher dispersion. This effect was observed for HTD catalysts by Böhm et al., where the supported catalysts performed better than unsupported particles from the same synthesis method.[8] However, Lettenmeier et al. discussed, whether activity increases for RS catalysts may also be the result of porous nanoparticles, which expose low-coordinated catalytic sites, presumably at Ir crystal defects and edges, that improve the catalysts' kinetic activity.[36] Since RS catalysts and Ir black show a similar onset potential, as shown in Figure 7b, the former explanation by Böhm is probably more likely since more active catalyst sites would result in a higher onset potential. Initially higher active sites, due to low-coordinated Ir may also be converted upon electrochemical oxidation to a hydrous IrO_x film during initial activation. The determination of actual electrochemically active surface area (ECSA) and concomitant comparison of different Ir species is ambiguous because different techniques for determination only apply to one Ir species. For example, CO-sorption experiments, which are readily applied for Pt-based catalysts, only apply for metallic Ir^0 species, which introduces uncertainties even for

catalysts that are mostly Ir^0 like RS and HTD.[37] These contain different additional amounts of Ir^{IV} which is not sensitive for CO-sorption and thus could lead to different ECSA estimations. Comparison to IrO_2 is also ambiguous since ECSA estimation cannot be done with the same technique as Ir^0. Additionally, measurements based on capacitance or IrO_2 cyclic voltammetry (CV) peak areas do not apply to support-based catalysts like the ones presented here, due to the contribution of capacitive currents from the support material.[37–41]

Similar performance at low potentials and an identical onset potential is displayed by the HTD catalyst, which is similar in chemical composition, as it is also made up of metallic Ir particles. A higher amount of Ir^{IV} in HTD compared to RS has seemingly no effect on catalyst performance. A possible explanation is the electrochemical oxidation of metallic Ir to a hydrous IrO_x surface film during the OER.[37] Ir^{IV} present in HTD in non-IrO_2 form could thus be indistinguishable in the in situ oxidized film. The only difference in electrochemical performance between the two catalysts occurs at higher potentials, where HTD experiences a steep decline in current, which could be caused by hindered mass transport. A plateauing of current normally hints at diffusion limitation, however, the curve shown for HTD could be explained by the blocking of active sites most likely due to the formation of product gas. Here, transport of oxygen is hindered and blockage of active sites
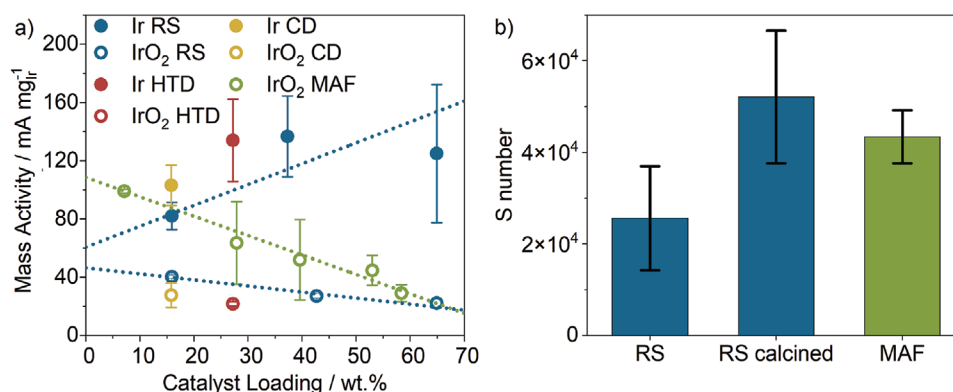
Figure 8. a) Mass activity regarding the catalysts' actual loading with (full) uncalcined catalysts and (hollow) calcined catalysts and b) stability number of the RS, calcined RS and MAF catalysts with nominal loadings of 65 wt% Ir.

**ADVANCED
SCIENCE NEWS**

www.advancedsciencenews.com

**ADVANCED
MATERIALS
INTERFACES**

www.advmatinterfaces.de

proliferates with higher potential and time as the product formation increases. Thus, the measured current decreases again at a higher potential. An additional difference to RS catalysts could be the lower electrical conductivity through the absence of a percolating network. Even though this mostly comes into effect at MEA level testing, it might have an influence here at higher currents.

The outlier here is again the CD method, with very low mass currents but also experiences the effect of decreasing current at high potentials. At low potentials, the activity of this catalyst is comparable to RS and HTD methods but performance declines sharply afterward. The difference between Ir species is apparent in a comparison of RS and Ir black to MAF catalyst, where the latter shows lower currents. Lower activity for IrO_2 is expected, but the MAF catalysts show only slightly lower performance than Ir black, positioning themselves as a better overall catalyst, due to the presumed higher stability. In comparison to calcined Ir catalysts, MAF seems superior as its activity is significantly higher. This could result from particle ripening for calcined catalysts, which experience a higher crystallization and probable higher particle size after thermal treatment, as discussed before. A higher amount of inactive Ir atoms due to decreased surface area thus decreases the mass-normalized current and activity. The decreased activity might also be a hint to complete surface oxidation of calcined catalysts since the accessibility of metallic Ir would improve the overall performance.[8,42] Complete surface oxidation would result in a core-shell-like structure for the RS method and this hypothesis is corroborated by the pre-activation CV shown in **Figure 9**a.

Here, the H_2 underpotential deposition is only present on metallic Ir^0.[20,37] With oxidation during CV scans this peak at around 0.1 to 0.3 V versus RHE shrinks in the uncalcined catalyst but is nonetheless present, which confirms the existence of accessible Ir^0 on the surface. After the activation procedure, this peak vanishes completely, which hints at complete surface oxidation to a hydrous IrO_x film, as depicted in Figure 9b. Upon calcination, this peak is also no longer present even in the first scan of the measurement, which proves the absence of accessible Ir^0 and thus corroborates a core-shell structure. The particles are thus present as metallic Ir^0 cores with a layer of Ir^{IV}, most likely as tetragonal IrO_2. A metallic Ir core was also

observed for an electrochemically oxidized metallic Ir catalyst, where the metal preservation is most likely due to metal-support interactions inhibiting the oxidation.[20,25] Higher amounts of Ir^{III} present in MAF catalysts might also explain its superior activity compared to calcined catalysts, which show negligible amounts of Ir^{III}. A surface hydroxide layer could therefore enhance the activity compared to more crystalline IrO_2 surfaces.[28] However, an increase of surface hydroxide species was also associated with a higher Ir dissolution rate and thus lower stability as the Ir-OH changes oxidation state from +III to +IV at OER potentials.[28]

Compared to commercial IrO_2, all calcined catalysts show similar mass-normalized performance. Especially at low overpotentials, those catalysts perform similarly with an onset potential of around 1.575 V versus RHE. The calcined CD catalysts display comparable mass currents to the other calcined catalysts, which is in stark contrast to the poor relative performance of the uncalcined catalyst. This difference could be caused by an incomplete reaction during the initial CD synthesis producing intermediate $Ir(OH)_4$, which is further converted to IrO_x or IrO_2 during the calcination.[43] A current maximum exhibited by the uncalcined HTD and CD catalysts disappears upon calcination for both, which could be caused by improved oxygen removal from active sites.

Overall, the catalysts presented here show very high activity, especially the MAF method IrO_2 catalysts. Regarding commercial state-of-the-art catalysts, the ones here perform as good or better both at low and high overpotentials. At low loadings, the MAF catalyst even exceeds the mass activity of the RS method, while presumably being more stable in OER conditions. In comparison to novel IrO_2-coated TiO_2 catalysts by Böhm et al. with the same method, the material here shows 996 A g_{Ir}^{-1} with 40 wt% compared to cited 1047 and 1048 A g_{Ir}^{-1} for 30 and 35 wt%, respectively.[7]

Most catalysts show a linear relationship between the mass-normalized activity and loading, which could be explained by dispersion of individual particles and thus higher available surface area.[25] Only RS shows an adverse trend, where the activity increases with 40 compared to 15 wt% Ir and decreases again or stays constant, considering fairly large error bars, at 65 wt% Ir. This optimum around 40 wt% could be the result
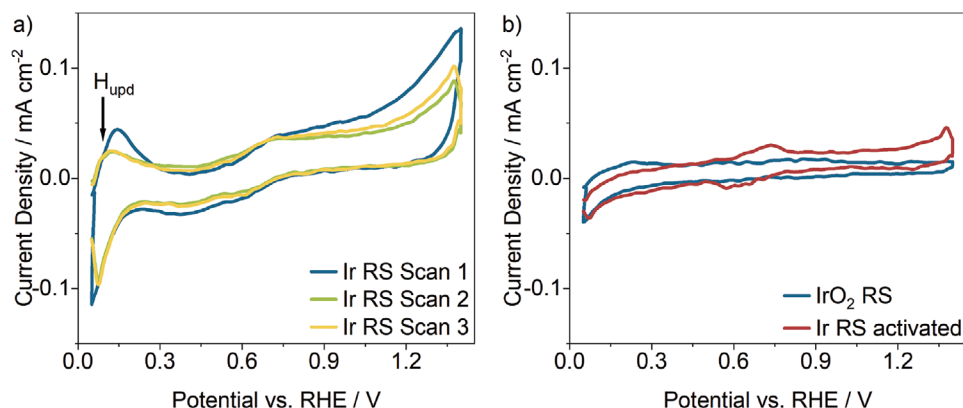
Figure 9. Cyclic voltammograms of a) 65 wt% Ir RS catalyst, during initial electrolyte immersion with first scans and b) 65 wt% Ir RS catalyst after activation and 65 wt% IrO_2 calcined RS catalyst.

ADVANCED
SCIENCE NEWS

www.advancedsciencenews.com

ADVANCED
MATERIALS
INTERFACES

www.advmatinterfaces.de

of a percolating network of Ir particles above 15 wt%, as seen in TEM micrographs before, which increases electric conductivity but leads to clustering of particles and thus could lower surface area at higher loadings. Even though patches of Ir particles can be observed at low loading, they might be too isolated to increase conductivity over the whole catalyst. Once this catalyst is calcined, the activity based on loading reverses back to the expected trend. This might be caused by particle ripening during thermal treatment as discussed earlier. The decreasing mass activity is however less pronounced compared to other catalysts but the overall mass activity is also lower compared to MAF catalysts.

Assessment of stability is non-trivial in an RDE setup and most likely not representative of stability in an MEA setup, since different processes occur, which alter the apparent stability parameters of the catalyst.[42] Lazaridis et al. recently reviewed the differences between RDE and MEA setups and concluded that an evaluation of stability is not representative in RDE, most likely due to micro-bubble formation on active sites.[42,44] Thus, higher potentials are exerted on other parts and different reversible degradation effects are present. Trogisch et al. also revisited this issue in more detail and concluded again that neither galvanostatic nor potentiostatic accelerated stress tests are suitable to assess the catalysts' stability in an RDE setup compared to actual stability in an MEA.[20] To provide a rough estimation of the stability difference between the calcined and uncalcined catalysts the S number was determined for both catalysts produced with the RS method and additionally for the MAF catalyst. The S number provides guidance that is rather independent of the type of catalyst, namely Ir or IrO_2, as it describes the ratio of produced O to dissolved Ir during the test and is thus widely applicable.[4,45] Figure 8b depicts the S number with its standard deviation across the three tested catalysts. It is widely accepted that IrO_2 is generally more stable than metallic Ir or IrO_x.[8,19,20,42] This can also be observed here, where the uncalcined RS catalysts show the lowest S number among those tested. Even though this catalyst had the highest activity during the stress test it also got dissolved more readily than those containing IrO_2. Its dissolution rate is about 10–20-fold higher than the other two which showed only a twofold difference. The calcined RS catalyst is apparently the overall most stable catalyst, which might be due to the difference in Ir^{III} species detected in XPS, which hints at the presence of IrO_x.[33] While the S number for the MAF catalyst is slightly lower than that of the calcined RS catalyst, during the stress test it showed a substantially higher O production rate, which hints at a positive trade-off between activity and stability. Overall the S number for these catalysts is in-line with results obtained by Daiane Ferreira da Silva et al., which showed an S number of around $2–4 \times 10^4$ for a mixture of IrO_2 and IrO_x.[4] The S number of the uncalcined RS catalyst even exceeds those with a comparable structure, most likely due to its high initial activity and thus high O production rate.

2.4. Evaluation of Synthesis Methods

In addition to different catalyst morphologies and specific Ir species, which influence the electrochemical performance, the overall evaluation of a catalyst synthesis also depends on the economic viability and scalability of reaction conditions. With the RS and MAF methods resulting in the desired loading and thus lower costly, superfluous Ir they already seem to be more viable than HTD and CD methods. The usage of synthesis solvents and other additives in the reaction also contributes to the viability of the method in addition to the deposition yield.

With MAF employing a salt melt using only readily available $NaNO_3$, this method can be easily adapted to industrial processes.[19] Catalyst properties like particle size and crystallinity are also easily modifiable by temperature variation. In contrast, the other methods employ a wet chemical approach that can increase complexity and may require the substitution of solvents or additives at high scales. With RS using ethanol as a solvent and CTAB as an additive, the materials are already widely used in research and industrial processes.[46,47] The usage of ethanol is not worrisome even at scale as it can be easily removed from the product through evaporation under reduced pressure and recirculated. Dry conditions due to $NaBH_4$ reduction may, nonetheless, require additional effort in synthesis and $NaBH_4$ is also toxic, which increases necessary precautions further.[48] The inert gas atmosphere could potentially be avoided since $NaBH_4$ is stable in alkaline conditions and thus the addition of some base may improve the accessibility of this method, however, the substitution for different reduction agents may be necessary.[49] The preparation of colloid suspensions for CD and HTD is more difficult to scale up as it employs ethylene glycol, which has a very high boiling point and thus prohibits easy removal under reduced pressure.[19,48] A different colloidal method could alleviate this problem, for example, the method proposed by Szeifert et al., which utilizes potassium superoxide with water as solvent.[8,50] HTD also requires a pressure vessel, which increases safety risks both on laboratory and industrial scales. In addition, all synthesis techniques except MAF produce Ir or IrO_x nanoparticles instead of IrO_2, which most likely requires post-synthesis oxidation as non-IrO_2 catalysts may not be stable for long-term use as different reaction pathways are facilitated.[8,19,51]

3. Conclusion

A comparison between different synthesis methods for Ir and IrO_2 was carried out to determine the viability of these methods for reliable production of Ir@ATO catalysts in research. In conclusion, the RS method was the most reliable in terms of accurate targetable deposition loading in addition to high electrochemical performance toward the OER. Performance-wise the HTD method proved to be equally suitable but lacked reproducible Ir loading, which might however be due to the formation of colloid before deposition. Considering IrO_2 catalysts, MAF showed reliably high deposition yields, when precursor impregnation is carried out diligently, in addition to very high performance, which supersedes both calcined RS and HTD catalysts. One main explanation for increased performance is good nanoparticle dispersion on the support, where calcined catalysts exhibit particle growth due to thermal treatment. CD method proved to provide low performance and deposition yield, which could be caused by some parameters like support surface area

**ADVANCED
SCIENCE NEWS**

www.advancedsciencenews.com

**ADVANCED
MATERIALS
INTERFACES**

www.advmatinterfaces.de

and thus is very dependent on specific conditions in the catalyst system investigated. Overall, RS and MAF methods may be the most reliable methods depending on the chemical composition of the targeted Ir species. They get complimented through fairly simple reaction procedures and easily scaled-up conditions.

4. Experimental Section

Synthesis: ATO particle synthesis was adapted from Hartig–Weiss et al.[25] In short, for a target dopant concentration of 5 wt% (Sb:Sn), Sb_2O_3 powder (1.1 mmol, 325.0 mg, Carl Roth), and Sn granules (42.25 mmol, 5.0 g, Carl Roth) were added to a mixture of concentrated HNO_3 (75.0 mL, 65 vol%, Carl Roth) and pure water (125.0 mL) in an 250 mL PTFE *DAB-2* autoclave liner (Berghof). After initial colloid formation, the autoclave was closed, heated to 140 °C, and held for 10 h. The resulting powder was then filtered and washed several times with pure water until neutral pH. Finally, the powder was calcined in air at 600 °C (3 °C min^{-1}) in a *P330* laboratory oven (Nabertherm) for 3 h and then ground in a mortar.

Reduction synthesis route employed an impregnation of ATO support with an Ir precursor and subsequent $NaBH_4$ reduction in inert gas atmosphere and was adapted from Wang et al.[24] Absolute ethanol (min. 99.9 vol%, CHEMSOLUTE) was first further purified with 3 Å molecular sieve (TH Geyer) for 3 days and stored in an inert gas atmosphere. In a typical synthesis for a nominal 40 wt% Ir catalyst, ATO (170 mg) was suspended in anhydrous ethanol (120.0 mL) and cetyltrimethylammonium bromide (CTAB, 4.82 mmol, 1.755 g, Carl Roth) was dissolved in the ATO suspension. The reaction mixture was then stirred for 30 min. Afterward, $IrCl_3 \times H_2O$ (0.59 mmol, 212 mg, Alfa Aesar) was dissolved in anhydrous ethanol (50.0 mL), added to the reaction mixture, and stirred overnight. For reduction, $NaBH_4$ (7.66 mmol, 290 mg, Sigma Aldrich) was dissolved in anhydrous ethanol (50.0 mL) and added drop-wise to the reaction mixture. During the reaction, the mixture was stirred for 4 h, separated by centrifuging (7000 rpm, 5 min, *Centrifuge 5430*, Eppendorf), and washed several times with pure water and absolute ethanol. The resulting black powder was finally dried in air at 70 °C.

MAF synthesis is based on the well-known oxidation method by Adams et al.[52] and carried out here adapted from a method by Böhm et al.[7] for Ir-based catalysts. For a nominal 40 wt% Ir catalyst, $IrCl_3 \times 3 H_2O$ (3.81 mmol, 137 mg) was mixed with ATO support (110 mg), with $NaNO_3$ (35.30 mmol, 3.0 g, Carl Roth), and pure water in a mass ratio of 1:12:24, respectively. The total mass of Ir and optionally ATO was kept constant to ensure sufficient ratios of oxidant to the precursor. The mixture was first stirred for 3 h and then sonicated to ensure fine dispersion of the educts. Afterward, it was transferred to a crystallizing dish and sonicated in an ultrasonic bath at 80 °C until the water evaporated. The resulting powder was ground and heated in air first at 150 °C (3 °C min^{-1}) for 2 h and then 375 °C (3 °C min^{-1}) for 1 h. The product was washed with pure water to remove $NaNO_3$ and dried in air at 70 °C. For reference purposes, the reaction was also carried out with commercial Ir black (1.30 mmol, 250 mg, *Ir mohr*, Umicore) as Ir precursor.

Colloidally dispersed Ir catalysts were synthesized via reduction in ethylene glycol analogous to Abbou et al.[26] For a nominal 40 wt% Ir catalyst, $H_2Cl_6Ir \times H_2O$ (0.147 mmol, 60 mg, CHEMPUR) was dissolved in pure water to result in a 6.95 mg$_{Ir}$ mL^{-1} solution. This solution (8.6 mL) was added to a mixture of ethylene glycol (120.0 mL, Carl Roth) and pure water (60.0 mL). Afterward, the pH was adjusted to 12 via the addition of a NaOH (0.5 м, AppliChem) solution of ethylene glycol and pure water in a 1:1 ratio, while the mixture turned from a deep brown to a pale-yellow color. The solution was then purged with Ar for 10 min and heated under reflux and Ar atmosphere to 160 °C for 4 h, after which it was passively cooled to room temperature.

For colloidally supported catalysts, ATO (43 mg) was dispersed in a 1:1 mixture of ethylene glycol and water (total volume 20 mL), and the Ir colloid was added. Finally, the pH was adjusted to one by the addition of a H_2SO_4 (1.0 м, Carl Roth) solution of ethylene glycol and pure water in a 1:1 ratio and left stirring for 3 days. The resulting suspension was then separated by centrifugation, washed several times with pure water, and dried in air at 70 °C.

Hydrothermally deposited Ir catalysts were synthesized according to a modified protocol by Böhm et al. with the same Ir colloid without ATO as described above.[8] ATO (160 mg) was suspended in pre-warmed tert-butanol (30 mL, Thermo Fisher Scientific) in a 250 mL PTFE autoclave liner. For a nominal 40 wt% Ir catalyst, 190 mL (0.147 mmol$_{Ir}$) of the previously prepared Ir colloid was added along with a stir bar and the autoclave was sealed. It was then kept stirring and heated to 175 °C for 12 h. After which the autoclave was cooled down to room temperature and the resulting powder was separated by centrifuging and washed with pure water several times. Finally, it was dried in static air at 70 °C.

Calcination of the synthesized Ir catalysts after synthesis to IrO_2 was adapted from Böhm et al.[7,8] Samples were heated in air in a laboratory oven at 375 °C (3 °C min^{-1}) and passively cooled to room temperature.

Characterization: RDE measurements were carried out in a glass cell that was cleaned overnight in a mixture of hydrogen peroxide and sulfuric acid. Afterward, it was rinsed with ample amounts of pure water and stored submerged in water between measurements. Catalyst suspension was prepared according to the procedure by Alia et al., by mixing catalyst powder (3.5 mg) with 2-propanol (2.4 mL, Carl Roth), pure water (7.6 mL), and Nafion solution (20 μL, 5 wt% in aliphatic alcohols, Sigma-Aldrich).[53] The suspension was then cooled in an ice bath and tip-sonicated for 30 min to ensure sufficient suspension. 10 μL were dropped on an 0.2475 cm^2 mirror-polished gold electrode (Pine Research) first at 100 rpm rotation, after application accelerated to 700 rpm, and then air dried. The prepared electrode was introduced to room-temperature argon-saturated sulfuric acid electrolyte (0.5 м, Carl Roth) and rotated at 2500 rpm in addition to a Pt-wire counter electrode, separated by a Luggin capillary, and a reversible H_2 (RHE) reference electrode. First, the catalyst was cycled 50 times from 1.2 to 1.8 V versus RHE with 100 mV s^{-1} after which an electrochemical impedance measurement was carried out at 0.35 V versus RHE, 10 mV amplitude, and a frequency range of 100 kHz to 0.1 Hz. Finally, three polarization curves were measured by linear sweep voltammetry in a range of 1.2 to 2.0 V versus RHE with 20 mV s^{-1}. In a separate measurement, CVs were recorded after the introduction of the electrode in the electrolyte at 0 V versus RHE, to avoid immediate Ir oxidation, from 0.05 to 1.4 V versus RHE with 10 mV s^{-1}. After three initial scans, the catalyst was activated, according to the protocol mentioned before, and then another three CV scans were carried out. All shown potentials were corrected for internal resistance by determination of the real impedance (Z') where imaginary impedance (Z'') is zero. In addition to the synthesized catalysts, commercial Ir black (*Ir mohr*, Umicore) and IrO_2 (*Elyst Ir75 048C*, Umicore) were evaluated as a reference.

For stability measurements, the catalyst suspension was created with double the concentration of the one above. Then the suspension was applied twice in 10 μL applications resulting in an overall volume of 20 μL. The measurement protocol for the accelerated stress test (AST) consisted of one EIS measurement at 0.6 V versus RHE, followed by a UI curve that was recorded by measuring three CV scans with a scan rate of 10 mV s^{-1} in a potential window between 1.2 and 1.8 V versus RHE. The durability test itself was adapted from Daiane Ferreira da Silva et al. and consisted of a galvanostatic hold at 3 mA, while the potential would not increase above 2.0 V versus RHE.[4] The S number was then calculated with the concentration of dissolved Ir in the electrolyte, determined through ICP-MS as described below and the generated amount of O, as described by Daiane Ferreira da Silva et al.[4]

XPS measurements were carried out on an *ESCALAB 250Xi* (Thermo Fisher Scientific) with a 1486.6 eV Al K$_\alpha$ source. Survey spectra were recorded with a pass energy of 10.0 eV, 50 ms dwell time, and a step size of 1 eV. High-resolution spectra were recorded with 50 eV pass energy, 50 ms dwell time, and a step size of 0.01 eV for Ir4f and 0.025 eV for other elements. Spectra fit was done in *Unifit* (Unifit Scientific

Software GmbH) and fitting parameters can be found in Table S1, Supporting Information.

X-ray powder diffraction measurements were carried out on an *EMPYREAN* diffractometer (PANalytical) in a Bragg–Bretano geometry with a Cu anode under 40 kV and 40 mA. For high-temperature XRD a *XRK900* stage was used under synthetic air flow. Measurements were taken after a 30 min dwell time at each temperature in 7 °C steps from 350 to 441 °C.

Nitrogen sorption measurements were carried out on a *Tristar II* (Micromeritics) at 77 K. First, the samples were outgassed at 80 °C for 16 h and then at 120 °C for 4 h to remove impurities and residual water. The specific surface area was determined by applying the Brunauer–Emmett–Teller (BET) formalism and for analysis of the pore size distribution, the density functional theory (DFT) model was employed.

ICP-MS measurements were carried out on a *XSERIES 2* spectrometer (Thermo Fisher Scientific). Before the measurement, 5 mg of the catalyst were digested with aqua regia (5.0 mL) in a PTFE-lined autoclave at 220 °C for 18 h and subsequently diluted with HNO_3 (2 vol%, ROTIPURAN Supra, Carl Roth) solution. For determination, an aliquot of diluted digestion was dosed with an internal Lu standard (Carl Roth).

TEM measurements were carried out on an *EM 900N* (Zeiss) operating at 80 kV and equipped with a W hairpin cathode. The catalyst was dispersed in ethanol and then deposited onto a *Formvar* 200 mesh polyvinyl formal-coated copper-grid (Plano) and dried in air for 10 min. High-resolution transmission (HR-TEM) electron microscopy measurements were carried out on a *JEM 2100F* (Jeol) operating at 200 kV and equipped with *Gatan Orius SC200D* and *Gatan Orius SC600* cameras. The sample preparation was analogous to TEM but the suspension was cast on a *Formvar* 300 mesh carbon-coated copper grid (Plano).

Supporting Information

Supporting Information is available from the Wiley Online Library or from the author.

Acknowledgements

Conflict of Interest

The authors declare no conflict of interest.

Data Availability Statement

The data that support the findings of this study are available from the corresponding author upon reasonable request.

Keywords

[1] U. Babic, M. Suermann, F. Büchi, L. Gubler, T. Schmidt, *J. Electrochem. Soc.* **2017**, *164*, F387.

[2] S. Shiva-Kumar, V. Himabindu, *Mater. Sci. Energy Technol.* **2019**, *2*, 442.

[3] C. van Pham, D. Escalera-López, K. Mayrhofer, S. Cherevko, S. Thiele, *Adv. Energy Mater.* **2021**, *11*, 2101998.

[4] C. D. Ferreira da Silva, F. Claudel, V. Martin, R. Chattot, S. Abbou, K. Kumar, I. Jiménez-Morales, S. Cavaliere, D. Jones, J. Rozière, L. Solà-Hernandez, C. Beauger, M. Faustini, J. Peron, B. Gilles, T. Encinas, L. Piccolo, F. H. Barros de Lima, L. Dubau, F. Maillard, *ACS Catal.* **2021**, *11*, 4107.

[5] U. Babic, E. Nilsson, A. Pătru, T. J. Schmidt, L. Gubler, *J. Electrochem. Soc.* **2019**, *166*, F214.

[6] M. Bernt, H. A. Gasteiger, *J. Electrochem. Soc.* **2016**, *163*, F3179.

[7] D. Böhm, M. Beetz, C. Gebauer, M. Bernt, J. Schröter, M. Kornherr, F. Zoller, T. Bein, D. Fattakhova-Rohlfing, *Appl. Mater. Today* **2021**, *24*, 101134.

[8] D. Böhm, M. Beetz, M. Schuster, K. Peters, A. G. Hufnagel, M. Döblinger, B. Böller, T. Bein, D. Fattakhova-Rohlfing, *Adv. Funct. Mater.* **2020**, *30*, 1906670.

[9] L. Ye, Y. Gao, S. Zhu, J. Zheng, P. Li, J. P. Zheng, *Int. J. Hydrogen Energy* **2017**, *42*, 7241.

[10] H. Ohno, S. Nohara, K. Kakinuma, M. Uchida, H. Uchida, *Catalysts* **2019**, *9*, 74.

[11] P. F. Karimi, B. Peppley, A. Bazylak, *ECS Trans.* **2015**, *69*, 87.

[12] K. Peters, P. Zeller, G. Stefanic, V. Skoromets, H. Němec, P. Kužel, D. Fattakhova-Rohlfing, *Chem. Mater.* **2015**, *27*, 1090.

[13] V. K. Puthiyapura, S. Pasupathi, H. Su, X. Liu, B. Pollet, K. Scott, *Int. J. Hydrogen Energy* **2014**, *39*, 1905.

[14] J. Xu, Q. Li, M. K. Hansen, E. Christensen, A. L. Tomás García, G. Liu, X. Wang, N. J. Bjerrum, *Int. J. Hydrogen Energy* **2012**, *37*, 18629.

[15] L. Solà-Hernández, F. Claudel, F. Maillard, C. Beauger, *Int. J. Hydrogen Energy* **2019**, *44*, 24331.

[16] V. A. Saveleva, L. Wang, O. Kasian, M. Batuk, J. Hadermann, J. J. Gallet, F. Bournel, N. Alonso-Vante, G. Ozouf, C. Beauger, K. J. J. Mayrhofer, S. Cherevko, A. S. Gago, K. A. Friedrich, S. Zafeiratos, E. R. Savinova, *ACS Catal.* **2020**, *10*, 2508.

[17] H.-S. Oh, H. N. Nong, T. Reier, A. Bergmann, M. Gliech, J. Ferreira de Araújo, E. Willinger, R. Schlögl, D. Teschner, P. Strasser, *J. Am. Chem. Soc.* **2016**, *138*, 12552.

[18] G. C. Silva, S. I. Venturini, S. Zhang, M. Löffler, C. Scheu, K. J. J. Mayrhofer, E. A. Ticianelli, S. Cherevko, *ChemElectroChem* **2020**, *7*, 2330.

[19] H. Dhawan, M. Secanell, N. Semagina, *Johnson Matthey Technol. Rev.* **2021**, *65*, 247.

[20] N. Trogisch, M. Koch, E. N. El Sawy, H. A. El-Sayed, *ACS Catal.* **2022**, *12*, 13715.

[21] C. Wang, F. Lan, Z. He, X. Xie, Y. Zhao, H. Hou, L. Guo, V. Murugadoss, H. Liu, Q. Shao, Q. Gao, T. Ding, R. Wei, Z. Guo, *ChemSusChem* **2019**, *12*, 1576.

[22] B. J. Kip, J. van Grondelle, J. Martens, R. Prins, *Appl. Catal.* **1986**, *26*, 353.

[23] M. Povia, D. F. Abbott, J. Herranz, A. Heinritz, D. Lebedev, B.-J. Kim, E. Fabbri, A. Patru, J. Kohlbrecher, R. Schäublin, M. Nachtegaal, C. Copéret, T. J. Schmidt, *Energy Environ. Sci.* **2019**, *12*, 3038.

[24] L. Wang, P. Lettenmeier, U. Golla-Schindler, P. Gazdzicki, N. A. Cañas, T. Morawietz, R. Hiesgen, S. S. Hosseiny, A. S. Gago, K. A. Friedrich, *Phys. Chem. Chem. Phys.* **2016**, *18*, 4487.

[25] A. Hartig-Weiss, M. Miller, H. Beyer, A. Schmitt, A. Siebel, A. T. S. Freiberg, H. A. Gasteiger, H. A. El-Sayed, *ACS Appl. Nano Mater.* **2020**, *3*, 2185.

[26] S. Abbou, R. Chattot, V. Martin, F. Claudel, L. Solà-Hernandez, C. Beauger, L. Dubau, F. Maillard, *ACS Catal.* **2020**, *10*, 7283.

[27] H.-S. Oh, H. N. Nong, T. Reier, M. Gliech, P. Strasser, *Chem. Sci.* **2015**, *6*, 3321.

[28] D. F. Abbott, D. Lebedev, K. Waltar, M. Povia, M. Nachtegaal, E. Fabbri, C. Copéret, T. J. Schmidt, *Chem. Mater.* **2016**, *28*, 6591.

[29] C. Felix, T. Maiyalagan, S. Pasupathi, B. Bladergroen, V. Linkov, *Micro Nanosyst.* **2016**, *4*, 186.

[30] S. Geiger, O. Kasian, B. R. Shrestha, A. M. Mingers, K. J. J. Mayrhofer, S. Cherevko, *J. Electrochem. Soc.* **2016**, *163*, F3132.

[31] D. Bernsmeier, M. Bernicke, R. Schmack, R. Sachse, B. Paul, A. Bergmann, P. Strasser, E. Ortel, R. Kraehnert, *ChemSusChem* **2018**, *11*, 2367.

[32] D. Gall, *J. Appl. Phys.* **2016**, *119*, 085101.

[33] V. Pfeifer, T. E. Jones, J. J. Velasco Vélez, C. Massué, R. Arrigo, D. Teschner, F. Girgsdies, M. Scherzer, M. T. Greiner, J. Allan, M. Hashagen, G. Weinberg, S. Piccinin, M. Hävecker, A. Knop-Gericke, R. Schlögl, *Surf. Interface Anal.* **2016**, *48*, 261.

[34] F. Claudel, L. Dubau, G. Berthomé, L. Sola-Hernandez, C. Beauger, L. Piccolo, F. Maillard, *ACS Catal.* **2019**, *9*, 4688.

[35] S. J. Freakley, J. Ruiz-Esquius, D. J. Morgan, *Surf. Interface Anal.* **2017**, *49*, 794.

[36] P. Lettenmeier, J. Majchel, L. Wang, V. A. Saveleva, S. Zafeiratos, E. R. Savinova, J.-J. Gallet, F. Bournel, A. S. Gago, K. A. Friedrich, *Chem. Sci.* **2018**, *9*, 3570.

[37] F. Bizzotto, J. Quinson, A. Zana, J. J. K. Kirkensgaard, A. Dworzak, M. Oezaslan, M. Arenz, *Catal. Sci. Technol.* **2019**, *9*, 6345.

[38] P. Connor, J. Schuch, B. Kaiser, W. Jaegermann, *Z. Phys. Chem.* **2020**, *234*, 979.

[39] S. Zhao, H. Yu, R. Maric, N. Danilovic, C. Capuano, K. Ayers, W. Mustain, *J. Electrochem. Soc.* **2015**, *162*, F1292.

[40] O. Reid, F. S. Saleh, E. B. Easton, *Electrochim. Acta* **2013**, *114*, 278.

[41] Y.-T. Kim, P. P. Lopes, S.-A. Park, A.-Y. Lee, J. Lim, H. Lee, S. Back, Y. Jung, N. Danilovic, V. Stamenkovic, J. Erlebacher, J. Snyder, N. M. Markovic, *Nat. Commun.* **2017**, *8*, 1449.

[42] T. Lazaridis, B. M. Stühmeier, H. A. Gasteiger, H. A. El-Sayed, *Nat. Catal.* **2022**, *5*, 363.

[43] Y. Zhao, E. A. Hernandez-Pagan, N. M. Vargas-Barbosa, J. L. Dysart, T. E. Mallouk, *J. Phys. Chem. Lett.* **2011**, *2*, 402.

[44] H. A. El-Sayed, A. Weiß, L. F. Olbrich, G. P. Putro, H. A. Gasteiger, *J. Electrochem. Soc.* **2019**, *166*, F458.

[45] S. Geiger, O. Kasian, M. Ledendecker, E. Pizzutilo, A. M. Mingers, W. T. Fu, O. Diaz-Morales, Z. Li, T. Oellers, L. Fruchter, A. Ludwig, K. J. J. Mayrhofer, M. T. M. Koper, S. Cherevko, *Nat. Catal.* **2018**, *1*, 508.

[46] J. García-Martínez, M. Johnson, J. Valla, K. Li, J. Y. Ying, *Catal. Sci. Technol.* **2012**, *2*, 987.

[47] N. A.-F. Aboul-Maaty, H. A.-S. Oraby, *Bull. Natl. Res. Cent.* **2019**, *43*, 25.

[48] J. Quinson, S. Neumann, T. Wannmacher, L. Kacenauskaite, M. Inaba, J. Bucher, F. Bizzotto, S. B. Simonsen, L. Theil Kuhn, D. Bujak, A. Zana, M. Arenz, S. Kunz, *Angew. Chem. Int. Ed.* **2018**, *57*, 12338.

[49] V. Minkina, S. Shabunya, V. Kalinin, V. Martynenko, A. Smirnova, *Int. J. Hydrogen Energy* **2008**, *33*, 5629.

[50] J. M. Szeifert, J. M. Feckl, D. Fattakhova-Rohlfing, Y. Liu, V. Kalousek, J. Rathousky, T. Bein, *J. Am. Chem. Soc.* **2010**, *132*, 12605.

[51] S. Siracusano, V. Baglio, S. A. Grigoriev, L. Merlo, V. N. Fateev, A. S. Aricò, *J. Power Sources* **2017**, *366*, 105.

[52] R. Adams, R. L. Shriner, *J. Am. Chem. Soc.* **1923**, *45*, 2171.

[53] S. M. Alia, G. C. Anderson, *J. Electrochem. Soc.* **2019**, *166*, F282.